Editors' Suggestion

Nondipole strong-field-approximation Hamiltonian

Simon Vendelbo Bylling Jensen, Mads Middelhede Lund, and Lars Bojer Madsen
Department of Physics and Astronomy, Aarhus University, DK-8000 Aarhus C, Denmark

(Received 19 February 2020; accepted 17 March 2020; published 17 April 2020)

We analyze the Hamiltonian of a charged particle in a strong external infrared laser pulse including nondipole effects to first order in $1/c$. We consider the corresponding classical equations of motions in the high-intensity, long-wavelength limit and identify for linearly polarized fields an accurate nondipole strong-field-approximation Hamiltonian. This Hamiltonian is expressed in a mixed gauge with separate light-matter interaction terms depending either on coordinate or momentum operators. It can be transformed into a nondipole velocity gauge and nondipole length gauge version. The associated beyond dipole Volkov states are given. Implications for laser-assisted scattering, strong-field ionization, laser-assisted photoeletric effect, and attosecond streaking are outlined.

DOI: 10.1103/PhysRevA.101.043408

I. INTRODUCTION

In the electric dipole approximation, the spatial variation of the external radiation field is neglected over the extent of the atomic or molecular quantum system. If photon absorption is considered in the linear regime, mathematically, then this simplification corresponds to replacing the propagation factor of light $\exp(i\boldsymbol{k}_L \cdot \boldsymbol{r})$ by unity. Here $\boldsymbol{k}_L$ is the wave vector specifying the laser propagation direction and with a magnitude of $k_L = \omega/c$, where ω is the angular frequency of the laser radiation and c is the speed of light. In the interaction with atoms and molecules, the initial state is described by a wave function, which is confined in space. If the spatial confinement of this initial state is such that effectively $i\boldsymbol{k}_L \cdot \boldsymbol{r} \ll 1$, then the dipole approximation is accurate. Corrections can be identified by considering a first-order expansion $\exp(i\boldsymbol{k}_L \cdot \boldsymbol{r}) \simeq 1 + i\boldsymbol{k}_L \cdot \boldsymbol{r}$, where the second term includes corrections of order $1/c$ and gives the electric quadrupole and magnetic dipole terms. It is clear that the dipole approximation breaks down in the high-frequency regime. For a recent example revealing nondipole effects in ionization in the perturbative XUV regime, see Ref. [1]. A typical signature of the breakdown of the dipole approximation is the lack of forward-backward symmetry with respect to the laser propagation direction; see also Ref. [2].

In a strong-field nonperturbative setting, nondipole effects were studied in connection with high-intensity, high-frequency ionization and the phenomenon of stabilization; see, e.g., Refs. [3–9]. The importance of the nondipole effects contained in the diamagnetic term proportional to the square of the vector potential in comparison to those contained in the term linear in the vector potential and the momentum operator was pointed out in connection with studies on high-intensity simulated Compton scattering [10] and Raman scattering [11]. General constraints on the applicability of the electric dipole approximation with respect to frequency and intensity were described in Refs. [12,13]. In these latter works, it was pointed out that the electric dipole approximation not only breaks down for high frequency but also for low frequency in the high-intensity regime. In simple terms this breakdown occurs because the laser-induced velocity, v, associated with the quiver motion scales as E_0/ω, with E_0 the field strength. This scaling means that in the limit of low frequency and high intensity, v/c can become nonnegligible and magnetic effects, expressed classical through the Lorentz force, can become important. The importance of nondipole effects in this limit was, e.g., stressed in connection with experimental work reporting an asymmetry of the electron momentum distribution at midinfrared wavelengths and intensities around $10^{14}\,\mathrm{W/cm^2}$ [14]. Such an asymmetry is a clear indication of a breakdown of the electric dipole approximation and had been observed before at near-infrared wavelengths [15]. Very recently, shifts along the laser propagation direction were found and analyzed in combined experimental and theoretical work [16,17]. These findings of nondipole effects in strong-field physics at infrared frequencies have renewed theoretical interest, and nondipole effects in this regime have, e.g., been considered in Refs. [18–30].

In this paper, we will be concerned with nondipole magnetic field effects of the order of v/c. We will consider the Hamiltonian for a charged particle in a molecular or atomic potential and an external field that is expanded to first order in $\boldsymbol{k}_L \cdot \boldsymbol{r}$. A consideration of the classical equations of motion and incorporation of typical strong-field-approximation ideas will lead to a nondipole strong-field-approximation Hamiltonian. This Hamiltonian separates position and momentum operators and was considered earlier at high frequency and high intensity without detailed classical justification [3,4,7]. With this Hamiltonian at hand, nondipole Volkov states are considered and nondipole effects for laser-assisted scattering, strong-field ionization, laser-assisted photoelectric effects, and attosecond streaking are considered.

II. RESULTS AND DISCUSSION

A. Nondipole Hamiltonian

Consider a particle with charge q (an electron has charge $q = -|e|$) in an external field described by the vector potential

$\boldsymbol{A}(\boldsymbol{r},t)$ and vanishing scalar potential. Let the field be elliptically polarized in the yz plane and let the propagation direction be along the x direction such that the vector potential can be expressed as a function of $\eta = \omega t - \omega x/c$, where ω is the angular frequency and c is the speed of light

$$\boldsymbol{A}(\boldsymbol{r},t) = A_0(\eta)\begin{pmatrix} 0 \\ \epsilon\cos(\eta) \\ \sin(\eta)\end{pmatrix}, \tag{1}$$

where $A_0(\eta)$ is an envelope function describing the temporal and spatial shape of the pulse. The parameter $\epsilon \in [0;1]$ describes the degree of polarization of the pulse. For example, if $\epsilon = 0$ or $\epsilon = 1$, then the pulse is linearly or circularly polarized, respectively. The amplitude of the vector potential envelope function relates to the intensity through the Poyntings vector and therefore depends on the ellipticity. In atomic units one could use for the vector potential amplitude $(\sqrt{I}/\omega)/\sqrt{1+\epsilon^2}$, where I is the intensity.

In the nondipole approximation, the center of mass and relative motions do not decouple. We consider a case where a light particle, say, an electron, moves in the potential of a much heavier particle—a nucleus. In this case it is accurate to assume that the center of mass stays at rest and all the momentum is absorbed by the lighter particle. The Hamiltonian for this latter particle of mass m for a vanishing scalar potential is obtained by minimal coupling, $\boldsymbol{p} \to \boldsymbol{p} - q\boldsymbol{A}(\eta)$, and given explicitly by

$$H(t) = \frac{[\boldsymbol{p} - q\boldsymbol{A}(\eta)]^2}{2m} + V(\boldsymbol{r}), \tag{2}$$

where $V(\boldsymbol{r})$ is the atomic or molecular potential. A Taylor expansion of the vector potential Eq. (1) to first order in $1/c$ gives the vector potential $\boldsymbol{A}^{(01)}(\eta) = \boldsymbol{A}(\eta)|_{\eta=\omega t} - (\omega x/c)\partial_\eta \boldsymbol{A}(\eta)|_{\eta=\omega t}$. We introduce the following notation:

$$\boldsymbol{A}^{(01)}(\eta) = \boldsymbol{A}^{(0)}(t) + \boldsymbol{A}^{(1)}(\eta), \tag{3}$$

with the familiar dipole term

$$\boldsymbol{A}^{(0)}(t) = A_0(t)\begin{pmatrix} 0 \\ \epsilon\cos(\omega t) \\ \sin(\omega t)\end{pmatrix} \tag{4}$$

and with a term that depends linearly on the coordinate in the propagation direction

$$\boldsymbol{A}^{(1)}(\eta) = \boldsymbol{A}_c^{(1)}(\eta) + \boldsymbol{A}_e^{(1)}(\eta), \tag{5}$$

where the first term with subscript c comes from the carrier variation of $\boldsymbol{A}(\eta)$,

$$\boldsymbol{A}_c^{(1)}(\eta) = A_0(t)\begin{pmatrix} 0 \\ \epsilon x(\omega/c)\sin(\omega t) \\ -x(\omega/c)\cos(\omega t)\end{pmatrix}, \tag{6}$$

and the second term with subscript e in Eq. (5) comes from the variation of the envelope,

$$\boldsymbol{A}_e^{(1)}(\eta) = -[\partial_\eta A_0(\eta)|_{\eta=\omega t}]\begin{pmatrix} 0 \\ \epsilon x(\omega/c)\cos(\omega t) \\ x(\omega/c)\sin(\omega t)\end{pmatrix}. \tag{7}$$

As soon as the pulse contains more than, say, 6 or 7 cycles, the contribution to $\boldsymbol{A}^{(1)}(\eta)$ due to the variation of the envelope [Eq. (7)] is much smaller than the contribution from Eq. (6) [31]. This is the situation we will focus on in this work, and we refer to this regime as the long-pulse limit, even though the pulse may only contain, say, 10 cycles. Inserting Eq. (3) into Eq. (2), keeping terms up to and including $1/c$, working in the Coulomb gauge and suppressing the arguments of H, $\boldsymbol{A}^{(0)}$, $\boldsymbol{A}^{(1)}$ and V for notational convenience, leads to

$$H = \frac{[\boldsymbol{p} - q\boldsymbol{A}^{(0)}]^2}{2m} - \frac{q}{m}\boldsymbol{A}^{(1)}\cdot\boldsymbol{p} + \frac{q^2}{m}\boldsymbol{A}^{(0)}\cdot\boldsymbol{A}^{(1)} + V. \tag{8}$$

We verify the relation $\boldsymbol{A}^{(1)} = (x/c)\boldsymbol{E}^{(0)}$, with $\boldsymbol{E}^{(0)} = -\partial_t \boldsymbol{A}^{(0)}$ and the Hamiltonian in Eq. (8) can be expressed as

$$H = \frac{[\boldsymbol{p} - q\boldsymbol{A}^{(0)}]^2}{2m} + \frac{x}{c}\left(\frac{q^2}{m}\boldsymbol{A}^{(0)} - \frac{q}{m}\boldsymbol{p}\right)\cdot\boldsymbol{E}^{(0)} + V, \tag{9}$$

which is the form recently considered in strong-field applications [26,27,29]. Effects of changing the carrier envelope phase, $\phi_{\rm CEP}$, can easily be addressed by the substitution $\omega t \to \omega t + \phi_{\rm CEP}$ in the expressions for the vector potential.

The Hamiltonians of Eqs. (8) and (9) contain terms that depend on the product of x and p_z. This product complicates the practical numerical solution of the corresponding time-dependent Schrödinger equation (TDSE). For example, the TDSE cannot be readily propagated with the standard split-step fast Fourier method [32], which relies on propagating operators that are solely functions of spatial coordinates in coordinate space and operators that are solely functions of momentum coordinates in momentum space. An elegant solution to this problem was recently considered in Ref. [27] by application of a unitary operator involving a product between coordinate and momentum operators. However, the dependence of this unitary operator on the generator of translations, the momentum operator $\boldsymbol{p}$, leads to a time-dependent displacement of the spatial coordinate of the potential, which complicates the propagation of the TDSE and would be advantageous to avoid. It would be convenient to introduce accurate approximations that bring the Hamiltonian on a form, which does not mix the operators and avoids an introduction of a time dependence of the atomic or molecular potential. This is what we seek to do in the following.

B. Classical equations of motion

To proceed it is helpful to consider the classical equations of motions corresponding to the Hamiltonians in Eqs. (2) and (8). Hamilton's classical equations of motion give of course the same result as a direct consideration of the Lorentz force. Keeping full retardation, the equation of motion reads

$$m\ddot{\boldsymbol{r}} = q(\boldsymbol{E} + \dot{\boldsymbol{r}}\times\boldsymbol{B}) - \nabla V, \tag{10}$$

with $\boldsymbol{B} = \nabla\times\boldsymbol{A}$ and $\boldsymbol{E} = -\partial_t\boldsymbol{A}$ and $\boldsymbol{A}$ given by Eq. (1).

The result reads to leading order in $1/c$

$$m\ddot{\boldsymbol{r}} = q(\boldsymbol{E}^{(01)} + \dot{\boldsymbol{r}}\times\boldsymbol{B}^{(1)}) - \nabla V, \tag{11}$$

with $\boldsymbol{E}^{(01)} = -\partial_t\boldsymbol{A}^{(01)}$ the electric field corresponding to the leading order in $1/c$ expansion $\boldsymbol{A}^{(01)}$ given by Eq. (3) and $\boldsymbol{B}^{(1)} = \nabla\times\boldsymbol{A}^{(1)} = \boldsymbol{B}_c^{(1)} + \boldsymbol{B}_e^{(1)}$ the spatially independent B-field component obtained from the vector potential in Eq. (5)

given explicitly by

$$\boldsymbol{B}_c^{(1)} = A_0(t)\begin{pmatrix} 0 \\ (\omega/c)\cos(\omega t) \\ \epsilon(\omega/c)\sin(\omega t) \end{pmatrix} \tag{12}$$

and

$$\boldsymbol{B}_e^{(1)} = -(\partial_\eta A_0(\eta)|_{\eta=\omega t})\begin{pmatrix} 0 \\ -(\omega/c)\sin(\omega t) \\ \epsilon(\omega/c)\cos(\omega t) \end{pmatrix}. \tag{13}$$

Introducing ideas from strong-field physics

Much of strong-field physics has been explained by considering the motion of electrons in the continuum and by either neglecting the effect of the potential V, as in the simple man model [33–37] or treating it perturbatively along the trajectories induced by the external field (see, e.g., Refs. [38,39]). We are interested in a regime where the laser intensity is large and the frequency is small. It makes sense to consider the effect of the B-field component along the E-field-induced motion; i.e., we are led to the consideration of the approximate equations of motion,

$$m\ddot{x} = q\big(\dot{y}B_z^{(1)} - \dot{z}B_y^{(1)}\big), \tag{14}$$

$$m\ddot{y} = q\big(-\partial_t A_y^{(0)}\big), \tag{15}$$

$$m\ddot{z} = q\big(-\partial_t A_z^{(0)}\big), \tag{16}$$

where we consider the dominant dipole part of the E-field and express the force in terms of the relevant vector potential. The y and z components of Eqs. (15) and (16) are readily integrated to give the laser-induced velocity in the polarization plane, $\dot{y} = (-q/m)A_y^{(0)}$ and $\dot{z} = (-q/m)A_z^{(0)}$, i.e.,

$$\dot{\boldsymbol{r}} = \dot{\boldsymbol{r}}_D = (-q/m)\boldsymbol{A}^{(0)}. \tag{17}$$

A subscript D indicates that the velocity is obtained from the dipole field alone. To proceed, we consider the long-pulse limit, where the contribution from Eq. (13) can be neglected compared with the contribution from Eq. (12). Inserting the expression of Eq. (17) into Eq. (14) gives the following equation of motion in the pulse propagation direction:

$$m\ddot{x} = q\big(\dot{y}_D B_z^{(1)} - \dot{z}_D B_y^{(1)}\big)[1 - \delta(\epsilon, 1)]. \tag{18}$$

On the right-hand side of Eq. (18), we multiply by the factor $[1 - \delta(\epsilon, 1)]$, which, as explained below, is inserted to remind us that the considered force in this approximation and long-pulse limit is zero for circularly polarized fields, $\epsilon = 1$. This can be verified in the long-pulse limit by the expressions for the velocities and B-field components given above. Physically, the absence of such a force for circularly polarized light can easily be understood by noting that for circularly polarized light the direction of the vector potential is perpendicular to the electric field direction. Hence, the B field and the vector potential are parallel or antiparallel and since the laser-induced dipole velocity is proportional to the vector potential [see Eq. (17)], the Lorentz force associated with the laser-induced dipole motion in circularly polarized field is vanishing in the present approach for the long-pulse limit due to the vanishing cross products between parallel vectors.

For linear polarization the situation is quite opposite. In this case, the vector potential and the E field are parallel or antiparallel and therefore the vector potential, and hence the laser-induced dipole velocity [see Eq. (17)], is perpendicular to the B field, which maximizes the cross product of the Lorentz force.

To see clearly that the nondipole term induces a radiation pressurelike force in the propagation direction, we note that the right-hand side of Eq. (18) can be rewritten to give

$$m\ddot{x} = (q^2/2mc)\partial_t[(\boldsymbol{A}^{(0)})^2][1 - \delta(\epsilon, 1)], \tag{19}$$

which clearly displays the positive sign of the force in the propagation direction. Equation (19) can be integrated to give a positive velocity in the propagation direction,

$$\dot{x} = \frac{q^2}{2m^2c}(\boldsymbol{A}^{(0)})^2[1 - \delta(\epsilon, 1)]. \tag{20}$$

The integration of Eqs. (14)–(16) with $\dot{\boldsymbol{r}}_D$ from Eq. (17) accounts for the effect of the B field along the trajectory induced by the laser in the polarization direction (plane) corresponding to the equations of motion,

$$m\ddot{\boldsymbol{r}} = q\{(-\partial_t \boldsymbol{A}^{(0)}) + \dot{\boldsymbol{r}}_D \times \boldsymbol{B}^{(1)}[1 - \delta(\epsilon, 1)]\}. \tag{21}$$

To conclude this section, we note that the idea of accounting for the Lorentz force along the trajectory induced by the dipole motion leads to the equations of motion in Eq. (21). We also note that in the long-pulse limit, this contribution to the nondipole effects is a decreasing function of the ellipticity of light. For circularly polarized light, there is no Lorentz force in the long-pulse limit with this approach. In linearly polarized fields, this contribution to the nondipole effects is maximized, since in this case the laser-induced motion is perpendicular to the direction of the magnetic field. These observations stress the sensitivity of nondipole effects to the polarization of the driving light.

C. Illustrative calculations

We saw in Sec. II B that the nondipole effects captured by accounting for the Lorentz force only along the laser-induced dipole trajectory is maximized for linearly polarized light in the long-pulse limit. We therefore expect the present strong-field-inspired approach to be most accurate for linearly polarized fields. For this reason, we will focus on linearly polarized light in the illustrations given in this section. We have performed several other simulations with polarizations from linear to circular by increasing ϵ and as expected the quality of the approximation decreases with increasing ϵ.

Figure 1 shows an example for an electron for a set of laser parameters similar to those used in a recent experiment reporting nondipole effects in the photoelectron momentum distribution with intense long-wavelength light [14] (see the caption of Fig. 1 for laser parameters). The excursion perpendicular to the polarization direction in the nondipole-induced figure-of-eight motion of the free electron is $\simeq 1$ for the chosen parameters and hence marks the onset of low-frequency nondipole effects [12,13]. In the experiments of Refs. [14–17] nondipole effects were identified by a shift

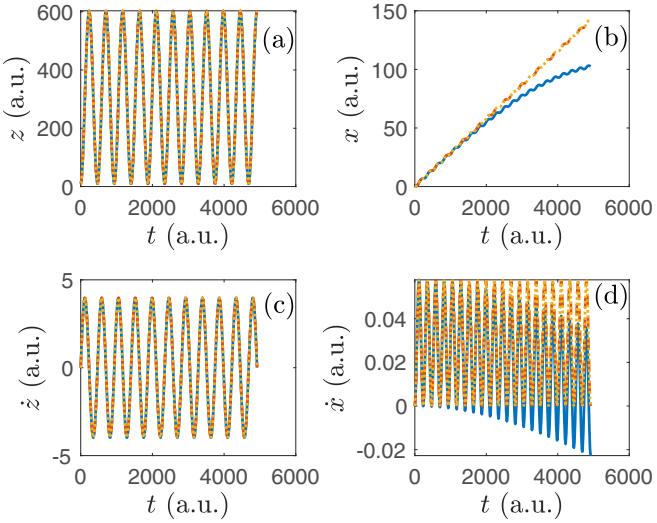

FIG. 1. (a) Position in atomic units (a.u.) of an electron in the laser polarization direction as a function of time, t in a.u., (b) position of an electron in a.u. in the laser propagation direction as a function of time, (c) velocity of an electron in a.u. in the laser polarization direction as a function of time, (d) velocity of an electron in a.u. in the laser propagation direction as a function of time. The wavelength of the laser field is $\lambda = 3.4\,\mu$m and the intensity is 1×10^{14} W/cm^2. The propagation time in a.u. corresponds to 10.5 cycles of the field. The intensity corresponds to an intensity of 0.0028 a.u. The long dashed (red) curves show the results considering the effect of the B field along the trajectory induced along the polarization direction corresponding to Eq. (21), the full (blue) curves show the results obtained by including nondipole effect to leading order in $1/c$ Eq. (11) but without the effect of the potential V, the dotted (yellow) curves show the result with full inclusion of nondipole effects, i.e., with full spatial dependence in E and B fields, Eq. (10), but without the potential V.

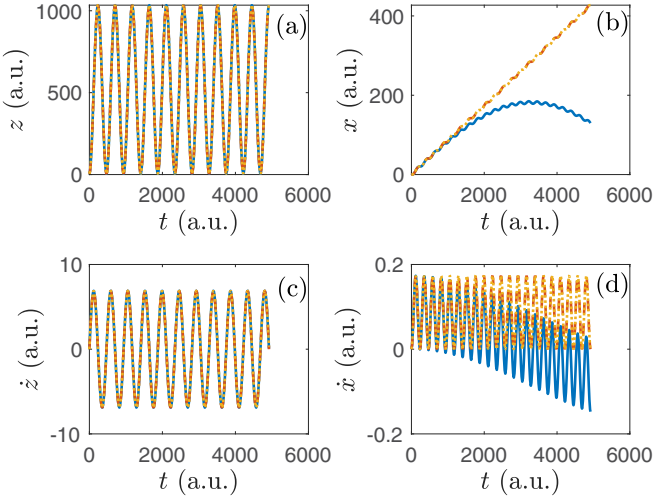

FIG. 2. As described in the caption of Fig. 1 but for an intensity of 3×10^{14} W/cm^2, corresponding to 0.0085 a.u.

of the photoelectron momentum distribution along the propagation direction. In the results shown in the figure, the trajectories start at the peak of the E-field at the exit point $(0, 0, z_0)$, $z_0 = I_p/E_0$ with $I_p = 0.5$ a.u. for atomic hydrogen and with zero initial velocity. They propagate for 10.5 cycles of the field with the Coulomb force neglected. The figure shows that the results obtained from integrating the equations of motion with full retardation Eq. (10) (but without V in this case) and the results obtained by including the effect of the B field perturbatively along the E-field-induced motion as in Eq. (21) are identical. In the figure, we also show results including the effect of retardation to the conventional first order in $\omega x/c$, i.e., from Eq. (11) again without the force from the potential V. In this case, we see a deviation from the exact result and the result of Eq. (21) in the propagation direction. This poor performance of the equations of motion corresponding to the $1/c$ expansion is due to the presence of the $\boldsymbol{E}^{(01)}$ term in Eq. (11), which includes terms linear in x. These terms are not small when x is large and leads to a breakdown of the expansion as expected. It is interesting to note that the results obtained from Eq. (21) do not suffer from this shortcoming. Figure 2 shows results as Fig. 1, but for a higher intensity and the conclusions are the same. Since the considered parameters are characteristic for the values that can be explored experimentally, and the agreement between the exact [of Eq. (10)] and the approximate [of Eq. (21)] treatment is excellent, we conclude that a perturbative treatment of the magnetic field along the E-field-induced trajectories is accurate in the absence of any atomic or molecular potential. We also conclude that the conventional expansion to $1/c$ [Eq. (11)] may be problematic due to a nonvanishing contribution from a force related to the spatial dependence of the E-field that is not present in the exact treatment and neither in the approximation of Eq. (21).

To illustrate the effect of an attractive potential on the classical trajectories, we show results in Fig. 3 for the case of the presence of an attractive Coulomb potential corresponding

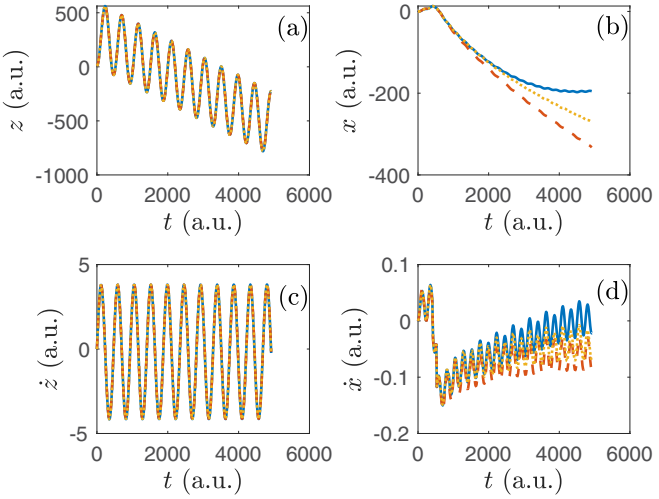

FIG. 3. As described in the caption of Fig. 1 but now including the effect of the Coulomb potential in the equations of motion, i.e., the effect of the force $-\nabla V$, with $V = -e^2/[(4\pi\epsilon_0)r]$. Compared with the exact result, we see a deviation in the electron (b) position and (d) velocity along the propagation direction for the nondipole strong-field-approximation trajectories in the presence of the Coulomb potential. This deviation is not worse than that of the standard $1/c$ expansion.

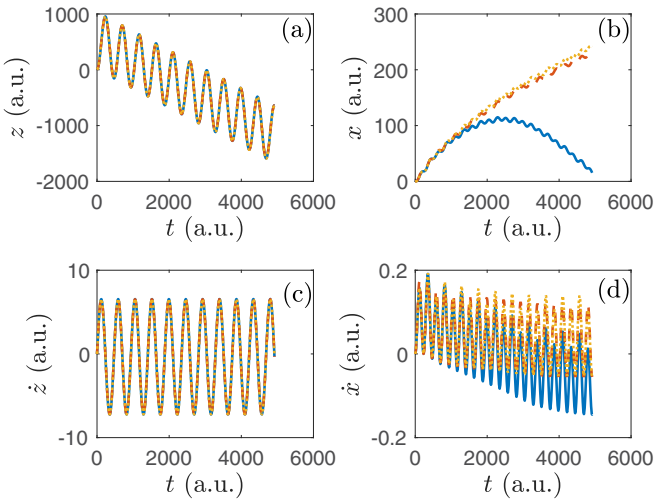

FIG. 4. As described in the caption of Fig. 3 but for an intensity of 3×10^{14} W/cm^2, corresponding to 0.0085 a.u.

to ionization of the hydrogen atom. The trajectories are propagated as in Fig. 1 but now including the force terms from the attractive Coulomb potential on the electron. In the considered nondipole cases, there is no need to soften the Coulomb potential since the Lorentz force induces a motion along the propagation direction x such that the x values are typically nonvanishing at the instants when $z = 0$, i.e., the trajectories do not probe the singularity at the origin to the same extent as in the dipole case for linearly polarized light. While the dynamics along the polarization direction is very accurately captured by a perturbative treatment of the effect of the B-field, a deviation sets in at around $t \sim 2000$ a.u. corresponding to ∼4 cycles in the position and velocity in the propagation direction. However, the perturbative treatment of the B field still captures the overall evolution of the position and the velocity. In fact, the performance of the approximation of Eq. (21) is not worse than the conventional $1/c$ expansion approach corresponding to Eq. (11). Compared with the potential-free case of Fig. 1, we note that the Coulomb potential can shift the effect of the radiation pressure and induce a net velocity and motion in the direction opposite to the propagation direction. This effect of the Coulomb potential was also found in other recent works [16,17,23] and pointed out by one of us some time ago (see Fig. 1 and the accompanying discussion in Ref. [40]). In Fig. 4, we show results as in Fig. 3, including the Coulomb potential, but for the higher intensity also considered in Fig. 2. We see that the performance of the approach of Eq. (21) is very good while the approach of Eq. (11) fails due to the reasons discussed above. As expected, the results in Figs. 3 and 4 show that the accuracy of the approximation of Eq. (21) improves as the laser intensity is increased. Of course, the considered equations of motion will eventually fail for intensities so high that v/c is no longer sufficiently small to justify a nonrelativistic treatment—but this is not the regime considered here.

To conclude this section, we note that the approximation described by a perturbative account of the nondipole B-field effect along the dipole laser-induced motion [Eq. (21)] is accurate in the regime of recent experiments for linearly polarized light. To connect to the quantum treatment, we therefore proceed in the next section with an identification of the corresponding Hamiltonian, i.e., an identification of the Hamiltonian that gives the equation of motion of Eq. (21) upon application of Hamilton's classical equations of motion.

D. Nondipole strong-field-approximation Hamiltonian

In the strong-field-approximation or Keldysh-Faisal-Reiss approach [41–43], the effect of the potential is neglected in the continuum. In the nondipole strong-field-approximation Hamiltonian, the idea is to account for the nondipole effects as captured by the classical equations of motion in Eq. (21). We are then lead to the search for the Hamiltonian that results in the equations of motion Eq. (21). It is left for the reader to verify, by applying the classical Hamilton equations that Eq. (21), with an additional force from the potential V, is obtained from the following nondipole strong-field-approximation Hamiltonian:

$$H^{\mathrm{SFA}}_{\mathrm{ND,MG}} = \frac{[\boldsymbol{p} - q\boldsymbol{A}^{(0)}]^2}{2m} + \frac{q^2}{m}\boldsymbol{A}^{(0)} \cdot \boldsymbol{A}^{(1)} + V, \tag{22}$$

i.e., by neglecting the term $(-q/m)\boldsymbol{A}^{(1)} \cdot \boldsymbol{p}$ compared with the $(q^2/m)\boldsymbol{A}^{(0)} \cdot \boldsymbol{A}^{(1)}$ term in Eq. (8). This Hamiltonian is the same as that considered in earlier work focusing on the high-intensity, high-frequency regime [3–9]. The superscript SFA in Eq. (22) reminds us that the Hamiltonian is inspired by strong-field physics ideas. The subscript ND indicates that this is a nondipole Hamiltonian.

It may be illustrative to rewrite the nondipole interaction term in Eq. (22) as

$$\frac{q^2}{m}\boldsymbol{A}^{(0)} \cdot \boldsymbol{A}^{(1)} = -q(\dot{\boldsymbol{r}}_D \times \boldsymbol{B}^{(1)}) \cdot \boldsymbol{r}, \tag{23}$$

which can be interpreted as the potential associated with the Lorentz force on the trajectory induced by the electric field in the polarization direction.

We note that $(q^2/m)\boldsymbol{A}^{(0)} \cdot \boldsymbol{A}^{(1)} = -q(\dot{\boldsymbol{r}}_D \times \boldsymbol{B}^{(1)}) \cdot \boldsymbol{r} = 0$ in the long-pulse limit for circularly polarized light. For circular polarization, $\epsilon = 1$, and in the long-pulse limit it is therefore the $-\frac{q}{m}\boldsymbol{A}^{(1)} \cdot \boldsymbol{p} = \frac{x}{c}(-\frac{q}{m}\boldsymbol{p}) \cdot \boldsymbol{E}^{(0)}$ terms from Eqs. (8) and (9) that are responsible for nondipole effects. Classically, this latter nondipole term gives a contribution to the Lorentz force in the plane of polarization due to motion in the propagation direction. The resulting velocity is not along the vector potential and therefore there is a nondipole effect. For linear polarization, however, it can be an accurate approximation to neglect these terms compared to the $(q^2/m)\boldsymbol{A}^{(0)} \cdot \boldsymbol{A}^{(1)}$ term as shown in Sec. II B. This sensitivity of the relevant nondipole terms to the polarization of light again means that different aspects of the nondipole effect can be probed in strong-field interactions with matter simply by changing the polarization from linear to circular. We remind the reader that focus in this work is on linear polarization where the approximation of Eq. (22) is expected to be most accurate based on the discussion in Secs. II B and II C.

The discussion of Secs. II B and II C led to the nondipole strong-field-approximation Hamiltonian, Eq. (22). This Hamiltonian, or unitarily transformed versions thereof, was considered in connection with calculations in the high-

intensity and high-frequency regime [3–9]. To the best of our knowledge it has not been considered in the long-wavelength limit in focus here nor has its accuracy been justified by classical analysis as that discussed in Sec. II B.

In Eq. (22) there is one interaction term proportional to the momentum operator and one interaction term proportional to the coordinate space operator. In strong-field physics, a Hamiltonian where the interaction with the external field is expressed by momentum (spatial coordinate) operators is often referred to as being in the velocity (length) gauge. Following that tradition, we refer to the Hamiltonian in Eq. (22) as being in a mixed velocity and length gauge (MG) representation, which explains the subscript. By applying unitary transformations to Eq. (22), it is possible to express all interactions with the external fields with either momentum or coordinate space operators. The explicit forms in the velocity and length gauges are given in the following sections.

1. Velocity gauge

To obtain the velocity gauge form of the nondipole strong-field-approximation Hamiltonian, we note that if the state $|\psi\rangle$ fulfils the TDSE $i\hbar\partial_t|\psi\rangle = H|\psi\rangle$, then the unitarily transformed state $|\psi'\rangle = U|\psi\rangle$ for a unitary operator U fulfills $i\hbar\partial_t|\psi'\rangle = H'|\psi'\rangle$ with

$$H' = UHU^\dagger + i\hbar\dot{U}U^\dagger. \tag{24}$$

In analogy with the operator $\exp(\frac{i}{\hbar}q\boldsymbol{A}^{(0)}\boldsymbol{r})$, with $-\partial_t\boldsymbol{A}^{(0)} = \boldsymbol{E}^{(0)}$, that facilitates the transformation between the length and velocity gauge forms in the dipole approximation, we introduce the temporal integral of the force factor in the propagation direction defined through the relation (excluding $\epsilon = 1$)

$$-\partial_t\boldsymbol{A}^{(M)} = \dot{\boldsymbol{r}}_D \times \boldsymbol{B}^{(1)}. \tag{25}$$

It is readily seen by using the Baker-Haussdorf lemma, $\exp(iG\lambda)A\exp(-iG\lambda) = A + i\lambda[G,A] + (i^2\lambda^2/2!)[G,[G,A]] + \cdots$, where G a Hermitian operator and λ is a real parameter [44], that a unitary transformation of Eq. (22) with

$$U = \exp\left(\frac{i}{\hbar}q\boldsymbol{A}^{(M)}\cdot\boldsymbol{r}\right) \tag{26}$$

leads to a transformed Hamiltonian with only momentum operators, i.e.,

$$H^{\mathrm{SFA}}_{\mathrm{ND,VG}} = \frac{(\boldsymbol{p} - q\boldsymbol{A}')^2}{2m} + V, \tag{27}$$

where

$$\boldsymbol{A}' = \boldsymbol{A}^{(0)} + \boldsymbol{A}^{(M)}, \tag{28}$$

with $\boldsymbol{A}^{(0)}$ given in Eq. (4) and having nonvanishing components in the plane of polarization and $\boldsymbol{A}^{(M)}$ defined in Eq. (25) and having a nonvanishing component along the propagation direction. The Hamiltonian in Eq. (27) is the nondipole strong-field-approximation Hamiltonian in the velocity gauge.

2. Length gauge

A nondipole strong-field-approximation length gauge Hamiltonian is obtained by unitary transforming the Hamiltonian in Eq. (27), according to Eq. (24), using the unitary operator

$$U = \exp\left(-\frac{i}{\hbar}q\boldsymbol{A}'\cdot\boldsymbol{r}\right). \tag{29}$$

The result can be obtained by using the Baker-Haussdorff lemma and it reads

$$H^{\mathrm{SFA}}_{\mathrm{ND,LG}} = \frac{\boldsymbol{p}^2}{2m} - q\boldsymbol{E}'\cdot\boldsymbol{r} + V, \tag{30}$$

where the effective electric field is defined as

$$\boldsymbol{E}' = -\partial_t\boldsymbol{A}', \tag{31}$$

with $\boldsymbol{A}'$ defined in Eq. (28).

E. Nondipole strong-field-approximation Volkov states

In strong-field physics, the Volkov wave states play a prominent role. These states are solutions to the TDSE in the absence of the atomic or molecular potential V. The solutions are readily found as follows.

The solution to the TDSE corresponding to the velocity gauge nondipole strong-field-approximation Hamiltonian of Eq. (27) is seen to be the velocity gauge nondipole strong-field-approximation Volkov state given by

$$\left|\psi^{V,\boldsymbol{k}}_{\mathrm{ND,VG}}\right\rangle = |\boldsymbol{k}\rangle e^{-\frac{i}{\hbar}S}, \tag{32}$$

with $\langle\boldsymbol{r}|\boldsymbol{k}\rangle = (2\pi)^{-3/2}\exp(i\boldsymbol{k}\cdot\boldsymbol{r})$ a plane wave with wave number $\boldsymbol{k}$, normalized such that $\langle\boldsymbol{k}'|\boldsymbol{k}\rangle = \delta(\boldsymbol{k}-\boldsymbol{k}')$. In Eq. (32), the nondipole strong-field-approximation Volkov phase is given by

$$S = \int_{-\infty}^{t}(\hbar\boldsymbol{k} - q\boldsymbol{A}')^2/(2m)dt'. \tag{33}$$

It then follows from Eq. (29) that the length gauge nondipole strong-field-approximation Volkov state, which solves the TDSE with the Hamiltonian in Eq. (30), is given by

$$\left|\psi^{V,\boldsymbol{k}}_{\mathrm{ND,LG}}\right\rangle = |\boldsymbol{k} - q\boldsymbol{A}'/\hbar\rangle e^{-\frac{i}{\hbar}S}. \tag{34}$$

Finally, we note that the mixed gauge nondipole state corresponding to the Hamiltonian in Eq. (22), by Eqs. (27) and (26), is given by

$$\left|\psi^{V,\boldsymbol{k}}_{\mathrm{ND,MG}}\right\rangle = |\boldsymbol{k} - q\boldsymbol{A}^{(M)}/\hbar\rangle e^{-\frac{i}{\hbar}S}. \tag{35}$$

Long-pulse limit

The above expressions for the nondipole Volkov states are on forms, which can be readily used in theory aiming at a description of charged particles with intense pulses of short duration, e.g., in strong-field ionization, and we come back to such applications of the nondipole Volkov state below. For the analysis of a certain class of strong-field physics problems, including the case of laser-assisted scattering, it is helpful to consider the long-pulse limit. In this limit the temporal envelope in the definition of the vector potential is neglected and it is assumed that the field is adiabatically switched on and off at suitably early and late times. In this case, $\boldsymbol{A}^{(M)}$ can be expressed as

$$\boldsymbol{A}^{(M)} = -\hat{\boldsymbol{x}}\frac{q}{2mc}(\boldsymbol{A}^{(0)})^2. \tag{36}$$

The integral in Eq. (33) can then be evaluated keeping terms up to order $1/c$ with the result (for $\epsilon = 0$ where the approach is most accurate)

$$S_{\rm lin} = \left(\frac{\hbar^2 k^2}{2m} + U_p'\right)t + \hbar \boldsymbol{k}\cdot\boldsymbol{\alpha}_0(t) - \frac{U_p'}{2\omega}\sin(2\omega t), \quad (37)$$

where

$$U_p' = \left(1 + \frac{\hbar k_x}{mc}\right)U_p \quad (38)$$

and

$$U_p = \frac{q^2 A_0^2}{4m} \quad (39)$$

is the ponderomotive potential describing the average energy of a free electron in the dipole field, and where

$$\boldsymbol{\alpha}_0(t) = \alpha_0 \cos(\omega t)\hat{\boldsymbol{z}}, \quad (40)$$

with $\hat{z}$ the direction of the linear polarization and where

$$\alpha_0 = \frac{qA_0}{m\omega} \quad (41)$$

is the classical quiver radius, i.e., the maximal excursion of the charged particle in the dipole field $\boldsymbol{A}^{(0)}$ of Eq. (4) with $\epsilon = 0$. We see from Eq. (38) that the nondipole contribution gives rise to a shift of the ponderomotive potential. The shift depends on the direction of the electron with respect to the propagation direction of the electromagnetic pulse. This shift is identical to the shift obtained by making a first-order Taylor expansion of the energy given on the right-hand side in Eq. (21) of Ref. [30].

The nondipole phase factor $e^{-\frac{i}{\hbar}S_{\rm lin}}$ entering the nondipole strong-field-approximation states can now be evaluated in terms of Bessel functions of integer order by using the generating functions $e^{ix\sin\phi} = \sum_n J_n(x)e^{in\phi}$, $e^{ix\cos\phi} = e^{ix\sin(\pi/2-\phi)} = \sum_n i^n J_n(x)e^{-in\phi}$, and $e^{ix\sin 2\phi} = \sum_n J_n(x)e^{i2n\phi}$. For linear polarization, we find an expression in terms of the generalized Bessel functions, $J_n(u, v)$ [43], and with the present choice of phase for the vector potential, the result reads

$$e^{-iS_{\rm lin}/\hbar} = \sum_n J_n\left(k_z\alpha_0, \frac{U_p'}{2\hbar\omega}\right)(-i)^n e^{-\frac{i}{\hbar}(\frac{\hbar^2k^2}{2m}+U_p'+n\hbar\omega)t}. \quad (42)$$

The factor in Eq. (42) can be combined with the suitable plane wave states of Eqs. (32), (34), and (35) to give the corresponding long-pulse limit expressions for the nondipole strong-field-approximation Volkov states.

F. Some physical effects of the nondipole contribution included in the nondipole strong-field-approximation Hamiltonian

The nondipole formalism considered here can be readily applied to strong-field physics in TDSE simulations and modeling. It should be stressed that the nondipole strong-field-approximation Hamiltonians are particularly well-suited for TDSE simulations since the Hamiltonians involve operators that are individually expressed either in coordinate or momentum space. Hence, they are on a form which readily allows for split-operator schemes [32]. To illustrate the usefulness of the present approach, we postpone the consideration of *ab initio* TDSE approaches, and here merely outline the nondipole theory for laser-assisted scattering and for nonperturbative strong-field ionization in their simplest possible formulations (see, e.g., Ref. [45] for corresponding calculations in the dipole case).

1. Nondipole strong-field-approximation laser-assisted scattering

In laser-assisted electron scattering (LAES), an electron scatters elastically by a potential in the presence of a laser pulse. The potential allows the electron to exchange energy with the assisting field in multiples of the photon energy. LAES is fundamental in recent advancements within ultrafast molecular imaging with laser-assisted electron diffraction [46,47] and is also a part of the foundation of strong-field physics, since the original LAES experiments gave the first clear demonstration of multiphoton free-free processes [48]. A theoretical description of LAES was formulated by Kroll and Watson in 1973 [49] and a description in the first-Born approximation for the scattering between the electron and the potential can be found in Ref. [50]. To make the discussion as simple as possible and to be able to clearly identify nondipole effects associated with the nondipole strong-field-approximation Hamiltonian, we consider laser-assisted scattering in linearly polarized light in the first-Born approximation. Using the nondipole strong-field-approximation velocity gauge Volkov states of Eq. (32), the S-matrix describing the transition from an initial state i with wave number $\boldsymbol{k}_i$, to a final state f with wave number $\boldsymbol{k}_f$ due to the scattering in the potential V, can be calculated. One finds in the first-Born approximation the following expression for the S-matrix:

$$(S-1)_{fi}^B = -i\int_{-\infty}^{\infty} dt \langle \psi_{\rm ND,VG}^{V,\boldsymbol{k}_f}|V|\psi_{\rm ND,VG}^{V,\boldsymbol{k}_i}\rangle. \quad (43)$$

We introduce the wave-number transfer vector, $\boldsymbol{Q} = \boldsymbol{k}_f - \boldsymbol{k}_i$, and the Fourier transform of the scattering potential, denoted by

$$\tilde{V}(\boldsymbol{Q}) = \frac{1}{(2\pi)^3}\int d\boldsymbol{r} e^{-i\boldsymbol{Q}\cdot\boldsymbol{r}}V(\boldsymbol{r}). \quad (44)$$

The nondipole strong-field-approximation Volkov phases form a Dirac delta function in energy upon integrating over time, which implies the following energy conservation relation for light linearly polarized in the z direction and propagating in the x direction:

$$\frac{\hbar^2 k_f^2}{2m} + \frac{\hbar \boldsymbol{k}_f\cdot\hat{\boldsymbol{x}}}{mc}U_p = \frac{\hbar^2 k_i^2}{2m} + \frac{\hbar \boldsymbol{k}_i\cdot\hat{\boldsymbol{x}}}{mc}U_p + l\hbar\omega. \quad (45)$$

Here l is the number of photons exchanged with the external field. As is clear from this equation $l > 0$ describes photon absorption and $l < 0$ describes photon emission. An additional effect of the nondipole term included in the nondipole strong-field approximation is the energy-contribution associated with the propagation direction $\hat{\boldsymbol{x}}$ of the field. Physically, these terms mean that the scattered electron will not only be able to gain photon energy from absorption or emission but also through a change in the direction of the scattered particle relative to the propagation direction. We express the time-dependent part of the nondipole strong-field approximation Volkov states by Eq. (42) and use the summation relations of

generalized Bessel functions [43], and we find the transition matrix elements $T_{fi}^{B}(l)$ for the scattering process as

$$(S-1)_{fi}^{B} = -2\pi\hbar i \sum_{l} T_{fi}^{B}(l), \tag{46}$$

$$T_{fi}^{B}(l) = (-i)^{l} J_{-l}\left(\boldsymbol{\alpha}_0 \cdot \boldsymbol{Q}, \frac{U_p}{2\omega mc}\boldsymbol{Q}\cdot\hat{\boldsymbol{x}}\right)\tilde{V}(\boldsymbol{Q}), \tag{47}$$

where $\boldsymbol{\alpha}_0 = \alpha_0\hat{\boldsymbol{z}}$ in the case of linearly polarized light. The influence of the laser on the scattering process is included in the generalized Bessel function in Eq. (47), which multiplies the field-free first-Born T-matrix, given by the Fourier transform of the potential in Eq. (44). The differential cross section is proportional to the norm square of the transition matrix element and we find that the nondipole laser-assisted scattering cross section of l-photon exchange can be expressed as

$$\frac{d\sigma^{\mathrm{B,ND}}(l)}{d\Omega}(\boldsymbol{k}_f(l), \boldsymbol{k}_i) = \frac{k_f(l)}{k_i} J_{-l}^{2}\left(\boldsymbol{\alpha}_0 \cdot \boldsymbol{Q}, \frac{U_p}{2\omega mc}\boldsymbol{Q}\cdot\hat{\boldsymbol{x}}\right)\frac{d\sigma^{\mathrm{B}}}{d\Omega}(\boldsymbol{k}_f(l), \boldsymbol{k}_i), \tag{48}$$

where the last factor on the right-hand side is the field-free cross section in the first-Born approximation. In the dipole approximation, the second argument of the generalized Bessel function in Eq. (48) vanishes, and since $J_l(x,0) = J_l(x)$, we have the following Born expression in the dipole approximation

$$\frac{d\sigma^{\mathrm{B,D}}(l)}{d\Omega}(\boldsymbol{k}(l), \boldsymbol{k}_i) = \frac{k_f(l)}{k_i} J_{-l}^{2}(\boldsymbol{\alpha}_0 \cdot \boldsymbol{Q})\frac{d\sigma^{\mathrm{B}}}{d\Omega}(\boldsymbol{k}_f(l), \boldsymbol{k}_i). \tag{49}$$

Comparing Eqs. (48) and (49), one sees that the nondipole effect is captured by the second argument in the generalized Bessel function. Due to the behavior of these functions, it follows that the nondipole effect is predicted to give a maximal contribution to the differential cross section in geometries, where the transfer vector, $\boldsymbol{Q}$, and the propagation direction of the light, $\hat{\boldsymbol{x}}$, are parallel or antiparallel, as well as for low photon frequencies, ω. This is exactly the domain where experiments found unexpected results and reported large disagreement with laser-assisted scattering theory formulated in the dipole approximation [51–56]. A significant feature of the nondipole strong-field-approximation approach is a lack of symmetry in the differential cross section around the polarization direction. This originates from the contribution in the propagation direction $\hat{\boldsymbol{x}}$ present in the nondipole and absent in the dipole case. Because of this contribution, by changing the laser propagation direction, the nondipole contribution may change from enhancing multiphoton absorption and suppressing multiphoton emission to the opposite. A more detailed investigation of the predictions of the nondipole strong-field-approximation Hamiltonian in connection with experimental data for laser-assisted scattering [51–53,55,56] is work for the future.

2. Nondipole strong-field-approximation multiphoton ionization

To see how the nondipole effects manifest themselves, it is useful first to consider again the long-pulse limit where the pulse is switched on and off at very early and late times. In the S-matrix formulation [43], the leading-order transition for multiphoton ionization reads in the nondipole case

$$(S-1)_{fi}^{B} = -i\int_{-\infty}^{\infty} dt \langle \psi_{\mathrm{ND,VG}}^{V,\boldsymbol{k}}| - \frac{q}{m}\boldsymbol{A}'\cdot\boldsymbol{p} + \frac{q^2\boldsymbol{A}'^2}{2m}|\phi_0\rangle, \tag{50}$$

where $|\psi_{\mathrm{ND,VG}}^{V,\boldsymbol{k}}\rangle$ is the time-dependent nondipole Volkov state of Eq. (32), $\boldsymbol{A}'$ is defined in Eq. (28), and $|\phi_0\rangle$ is the field-free initial state, which includes the trivial time dependence $e^{-\frac{i}{\hbar}E_b t}$ associated with the time evolution of the ground state with energy $E_b = -I_p$. Expressing the time-dependent part of the nondipole Volkov state by the expansion Eq. (42), the time integral is readily performed and the result reads

$$(S-1)_{fi}^{B} = -2\pi\hbar i \sum_{n_0} T_{fi}(\boldsymbol{k}_n), \tag{51}$$

with an energy conserving Dirac delta function giving the final kinetic energy as

$$\frac{\hbar^2 k_n^2}{2m} = n\hbar\omega - U_p' + E_b \tag{52}$$

for $n \geqslant n_0$ and n_0 the smallest number that makes the right-hand side of Eq. (52) positive. The T-matrix element in Eq. (51) to first order in $1/c$ reads

$$T_{fi}(\boldsymbol{k}_n) = (-i)^n (U_p' - n\hbar\omega) J_{-n}\left(\boldsymbol{\alpha}_0\cdot\boldsymbol{k}_n, \frac{U_p'}{2\hbar\omega}\right)\tilde{\phi}_0(\boldsymbol{k}_n), \tag{53}$$

with $\tilde{\phi}_0(\boldsymbol{k}_n) = (2\pi)^{-3/2}\int d\boldsymbol{r}\exp(-i\boldsymbol{k}_n\cdot\boldsymbol{r})\phi_0(\boldsymbol{r})$ the Fourier transform of the initial orbital evaluated at the momentum $\boldsymbol{k}_n$. The multiphoton ionization rate is related to the norm square of the transition matrix [43]. The energies of k_n for a given n depends on the component of $\boldsymbol{k}$ along the propagation direction $\hat{\boldsymbol{x}}$ due to the presence of U_p' of Eq. (38) in Eq. (52). This dependence induces an asymmetry in the photoelectron momentum distribution in the propagation direction: When the momentum of the photoelectron is along the propagation direction, U_p' is larger than when the directions are antiparallel. Note that the effect of the Coulomb force can change the momentum offset as illustrated in the classical simulations in Sec. II C. At a driving frequency of $\omega = 50$ a.u. and for intense fields, the nondipole strong-field approximation was shown to give qualitatively correct results for the photoelectron angular distributions when compared with TDSE results [9].

3. Nondipole-induced shift in the propagation direction

The nondipole effect manifests itself in the measured photoelectron momentum distribution, e.g., by a shift of this distribution along the laser propagation direction [14,15,17]. In the long-pulse limit the origin of this shift was discussed above. A saddle-point analysis can give a closed analytical expression for the estimation of the shift. The magnitude and direction of the shift depends on the polarization of light. It also depends on the relative strength of the laser field and the Coulomb potential, as illustrated by the examples in Sec. II C. An analytical estimate of the shift can be obtained by considering the leading-order term of the strong-field-ionization amplitude in the tunneling regime using the nondipole strong-field-approximation Hamiltonian as derived in detail in the Appendix. The result for the dominant contribution to the

nondipole-induced shift of the momentum distribution in the laser propagation direction is

$$(\hbar k_x)_{\rm shift} = \frac{1}{3c} I_p. \tag{54}$$

This shift was also found previously (see, e.g., Refs. [17–20]). It is encouraging that the shift is captured by the nondipole strong-field-approximation Hamiltonian. As noted above, the effect of the Coulomb potential can lead to a resulting net final drift of the outgoing low-energy electrons in the direction opposite to the laser propagation direction. To account for such effects in the S-matrix formulation, one would need to account for the atomic or molecular potential, V, in a more accurate manner, e.g., by developing the Born series to higher order in V, or integrating the effect of V along the laser-induced trajectory in an Eikonal-like approach.

4. Nondipole strong-field-approximation laser-assisted photoelectric effect and attosecond streaking

The nondipole strong-field-approximation Hamiltonian can also be used to include nondipole effects in an analysis of laser-assisted photoelectric effect (LAPE) (see, e.g., Ref. [57] for an experiment on LAPE) and attosecond streaking (see, e.g., Ref. [58]). In the LAPE case, the S-matrix to consider is

$$(S-1)^{B}_{fi} = -i \int_{-\infty}^{\infty} dt \langle \psi^{V,\boldsymbol{k}}_{\rm ND,VG}| - \frac{q}{m} \boldsymbol{A}_{\rm XUV} \cdot \boldsymbol{p} |\phi_0\rangle, \tag{55}$$

where $|\psi^{V,\boldsymbol{k}}_{\rm ND,VG}\rangle$ and $|\phi_0\rangle$ were defined after Eq. (50) and $\boldsymbol{A}_{\rm XUV}$ is the XUV field with the angular frequency $\omega_{\rm XUV}$ inducing single photon ionization. The nondipole effect is included in the nondipole Volkov wave function. Evaluation of the S matrix leads to an energy conservation relation

$$\frac{(\hbar k_n)^2}{2m} = \omega_{\rm XUV} - I_p - U'_p - n\hbar\omega \tag{56}$$

and a T-matrix element corresponding to n-photon exchange by the assisting IR given by

$$T_{fi}(\boldsymbol{k}_n) = (i)^n J_n\left(\boldsymbol{\alpha}_0 \cdot \boldsymbol{k}_n, \frac{U'_p}{2\hbar\omega}\right) \frac{(-q\boldsymbol{A}_{0,\rm XUV} \cdot \hbar\boldsymbol{k}_n)}{2m} \tilde{\phi}_0(\boldsymbol{k}_n), \tag{57}$$

where $\boldsymbol{\alpha}_0$ is the quiver radius associated with the assisting IR field and $\boldsymbol{A}_{0,\rm XUV}$ is the vector potential amplitude of the XUV field. The norm square of the T-matrix element gives the ionization rate. The nondipole effect is present in the modified ponderomotive energy U'_p given by Eq. (38).

For attosecond streaking, analysis based on the S matrix considered above, but for short pulses, can give an analytical estimate for the shift in the center of energy position due to nondipole effects. In the derivation, it is used that the nondipole Volkov phase changes only a little during the brief duration of the attosecond pulse, justifying a first-order Taylor expansion of the phase (see, e.g., Ref. [59] for the procedure). We find that the peak in the center of final (f) energy is determined by the relation

$$\frac{\hbar^2 k_f^2}{2m} + \frac{q^2 (\boldsymbol{A}^{(0)})^2}{2m} - \frac{q}{m} \boldsymbol{A}' \cdot \hbar\boldsymbol{k}_f + I_p - \hbar\omega_{\rm XUV} = 0, \tag{58}$$

where the vector potentials given by Eqs. (4) and (28) are evaluated at the time τ, when the attosecond XUV is fired w.r.t. the center of the femtosecond IR pulse. Using the explicit forms of the vector potentials introduced above, we find that a calculation for an IR field linearly polarized along the z direction and with propagation along the x direction gives rise to a shift in $\hbar k_{f,z}$ due to the $\boldsymbol{A}^{(M)}$ term present in $\boldsymbol{A}'$. The shift is described by the following substitution going from the dipole to the nondipole case:

$$\hbar k_{f,z} \to \hbar k_{f,z} - \frac{qA_0}{2mc} (\hbar k_{f,x}) \sin(\omega\tau). \tag{59}$$

We see from Eq. (59) that there is no nondipole effect, at the present level of theory, if the outgoing electrons are detected in the polarization direction (z). If the photoelectrons are detected at a nonvanishing angle w.r.t. the polarization direction, Eq. (59) shows that there is a nondipole-induced shift in the peak of the photoelectron energy distribution, which could be considered in the interpretation of attosecond time-delay experiments.

III. SUMMARY AND CONCLUSION

In this work, we have presented an analysis of nondipole effects to order $1/c$ in the nonrelativistic regime. The idea behind the approach is based in strong-field physics, where the effect of the strong-field driving along the laser polarization direction is of paramount importance. In this regime, often useful insights into electron dynamics can be obtained by accounting in an approximate manner for the interaction of the electron with the atomic or molecular potential. In line with these observations, we have explored to what extent it can be accurate to account for the effect of the B field along the laser-induced dipole motion. We have shown that while this particular nondipole effect can dominate and accurately describe nondipole effects for linearly polarized, high-intensity, infrared light, its contribution vanishes for circularly polarized light in the long-pulse limit. This analysis exposed the sensitivity of nondipole effects to the polarization of the driving light.

For high-intensity, infrared, linearly polarized light, it was shown by classical simulations that a perturbative description of the effect of the B field along the laser-induced dipole trajectories is accurate. Using Hamilton's classical equations of motion, we identified the corresponding classical Hamilton function and therefore also the quantum mechanical Hamiltonian. Because this Hamiltonian was obtained using ideas about the relative importance of interactions w.r.t. the dominant E-field interaction from strong-field physics, we refer to this Hamiltonian as the nondipole strong-field-approximation Hamiltonian. The Hamiltonian obtained in this way was previously applied to physics in the high-intensity, high-frequency regime [3–9], where in particular its numerical advantage was stressed. This Hamiltonian separates namely coordinate and momentum space operators in its mixed gauge version. This separation property is highly advantageous for numerical propagation schemes and allows us to formulate the light-matter interaction part of the Hamiltonian in terms of operators involving exclusively momentum space operators, or exclusively spatial coordinate space operators, corresponding

to the velocity gauge and the length gauge versions of the nondipole strong-field-approximation Hamiltonian.

With the nondipole strong-field-approximation Hamiltonian at hand we considered analytically some implications of nondipole effects on laser-assisted and laser-induced strong-field processes. The analytical approach was facilitated by the simple form of the Hamiltonian. In connection with laser-assisted scattering, we identified a maximal nondipole contribution to the cross section in scattering geometries where corresponding theory within the dipole approximation predicts a vanishing cross section. The nondipole strong-field-approximation Hamiltonian therefore seems a suitable starting point for developing theory in this geometry where the comparison between theory and experiment is still a problem to be dealt with. In connection with strong-field ionization, we identified laser-induced nondipole shifts of the maximum in the photoelectron momentum distribution. In the tunneling regime of small Keldysh parameter, we obtained an analytical expression for the dominant shift, which is in agreement with that obtained by others. We also outlined the nondipole effects induced by the nondipole strong-field-approximation Hamiltonian in related strong-field processes such as the laser-assisted photoelectric effect and attosecond streaking. In particular, we identified an additional nondipole-induced shift of the photoelectron energy distribution that could be considered in the interpretation of attosecond time-delay experiments.

In conclusion, we find that the nondipole strong-field-approximation Hamiltonian for linearly polarized light can be accurate in the low-frequency, high-intensity regime. We find that the Hamiltonian captures interesting nondipole effects already within the simplest analytical quantum mechanical approaches such as leading-order S matrix or strong-field-approximation theory. For these reasons, we think it is worthwhile to explore the predictions of this Hamiltonian in this regime in the future with, e.g., numerical *ab initio* methods, which would benefit from its non-space-and-momentum-mixing form, or with higher-order terms in laser-dressed Born-type expansions.

ACKNOWLEDGMENTS

We thank Morten Førre for useful discussions. This work was supported by the VKR center of excellence, QUSCOPE—Quantum Scale Optical Processes, and the Danish Council for Independent Research (Grants No. 7014-00092B and No. 9040-00001B).

APPENDIX: SADDLE-POINT ANALYSIS OF NONDIPOLE-INDUCED MOMENTUM SHIFT IN LASER PROPAGATION DIRECTION

When describing the process of recollision-free direct multiphoton ionization by S-matrix theory with an electromagnetic field in the electric dipole approximation, the photoelectron momentum distribution (PMD) will be symmetric around the laser propagation direction. In this Appendix, we derive an analytical result for the asymmetry induced in the PMD when the interaction with the electromagnetic field is described by the nondipole strong-field-approximation Hamiltonian. The relevant quantities, i.e., states and vector potentials, are given in the main text of the paper, but to make the derivation easier to follow, we make the presentation in this Appendix self-contained and reintroduce most quantities needed. To obtain an analytical estimate, we describe the electromagnetic field by the vector potential

$$\boldsymbol{A}' = \boldsymbol{A}^{(0)} + \boldsymbol{A}^{(M)}, \tag{A1}$$

with

$$\boldsymbol{A}^{(0)} = A_0 \sin(\omega t)\hat{\boldsymbol{z}} \quad \text{and} \quad \boldsymbol{A}^{(M)} = -\hat{\boldsymbol{x}}\frac{q}{2mc}(\boldsymbol{A}^{(0)})^2. \tag{A2}$$

The S-matrix to leading order reads

$$(S-1)^B_{fi} = -i\int_0^{t_f} dt \left\langle \psi^{V,\boldsymbol{k}}_{\mathrm{ND,VG}}\right| - \frac{q}{m}\boldsymbol{A}'\cdot\boldsymbol{p} + \frac{q^2\boldsymbol{A}'^2}{2m}\left|\phi_0\right\rangle, \tag{A3}$$

where the limits on the integral describe that we assume a main contribution to the amplitude to come from one dominant half cycle of the field. The nondipole strong-field-approximation velocity gauge Volkov state reads

$$\left|\psi^{V,\boldsymbol{k}}_{\mathrm{ND,VG}}\right\rangle = |\boldsymbol{k}\rangle\, e^{-\frac{i}{\hbar}S(t,\boldsymbol{k})}, \tag{A4}$$

with $\langle \boldsymbol{r}|\boldsymbol{k}\rangle = (2\pi)^{-3/2}\exp(i\boldsymbol{k}\cdot\boldsymbol{r})$ and the Volkov phase

$$\begin{aligned} S(t,\boldsymbol{k}) &= \int_0^t dt'(\hbar\boldsymbol{k} - q\boldsymbol{A}')^2/(2m) \\ &\approx \int_0^t dt'\left[\frac{(\hbar k)^2}{2m} - \frac{q}{m}\boldsymbol{A}^{(0)}\cdot(\hbar\boldsymbol{k}) \right. \\ &\quad \left. + \left(1+\frac{\hbar k_x}{mc}\right)\frac{(q\boldsymbol{A}^{(0)})^2}{2m}\right]. \end{aligned} \tag{A5}$$

The S-matrix element can be expressed as

$$(S-1)^B_{fi} = -i\int_0^{t_f} dt D(\boldsymbol{k},t) e^{\frac{i}{\hbar}S_{\mathrm{tot}}(t,\boldsymbol{k})}, \tag{A6}$$

where $D(\boldsymbol{k},t)$ describes the nonoscillating part of the integrand and S_{tot} is the total phase including the contribution from the time evolution of the ground state

$$\begin{aligned} S_{\mathrm{tot}}(t,\boldsymbol{k}) &= \int_0^t dt'\left[\frac{(\hbar k)^2}{2m} - \frac{q}{m}\boldsymbol{A}^{(0)}\cdot(\hbar\boldsymbol{k}) \right. \\ &\quad \left. + \left(1+\frac{\hbar k_x}{mc}\right)\frac{(q\boldsymbol{A}^{(0)})^2}{2m}\right] + I_p t. \end{aligned} \tag{A7}$$

Since the phase of Eq. (A7) is rapidly oscillating, the S-matrix element, Eq. (A6), can be approximated using the saddle-point approximation. The ionization probability for ionization and final electron momentum $\hbar\boldsymbol{k}$ is to leading-order in the interaction proportional to

$$P(\boldsymbol{k}) \propto e^{-2\mathrm{Im}[S_{\mathrm{tot}}(t_s,\boldsymbol{k})]}, \tag{A8}$$

where the saddle-point time, t_s, solves

$$\frac{\partial S_{\mathrm{tot}}(t,\boldsymbol{k})}{\partial t} = 0. \tag{A9}$$

The remaining task is to find t_s and use the approximate expression for the probability, Eq. (A8), to estimate the nondipole-induced shift of the PMD in the laser propagation direction.

The saddle-point equation to the zeroth order in $1/c$ reads

$$\frac{\partial S_{\rm tot}(t,\boldsymbol{k})}{\partial t} = 0 = \frac{(\hbar k)^2}{2m} - \frac{q}{m}A_0\sin(\omega t_s)\hbar k_z + \frac{q^2}{2m}A_0^2\sin^2(\omega t_s) + I_p. \tag{A10}$$

This equations is solved by

$$t_s = \frac{1}{\omega}\arcsin\left(\frac{\omega}{qE_0}\hbar k_z \pm i\gamma_{\rm eff}\right), \tag{A11}$$

where we have used $E_0 = \omega A_0$ and where $\gamma_{\rm eff} = \frac{\omega}{qE_0}\sqrt{\hbar^2k_x^2 + \hbar^2k_y^2 + 2mI_p}$ is a modified Keldysh factor. The standard Keldysh factor is given by $\gamma = \frac{\omega}{qE_0}\sqrt{2mI_p}$. Only the "+" solution in Eq. (A11) is used for the asymmetric shift-analysis of the PMD. One could include another saddle point $t_s + \pi/\omega$, corresponding to ionizing in the following half cycle. Including this extra saddle point would lead to interference effects in the PMD from the two ionization times. However, an analysis of the effect of using two saddle points leads to no significant difference in the nondipole-induced shift in the laser propagation direction of the PMD compared to only using a single saddle point. Therefore, the analysis of the asymmetry will be made using only the saddle point in Eq. (A10). Also note that the consideration of the saddle-point equation including the leading-order correction in $1/c$ will give the same final result, so it suffices to use the solution of Eq. (A11). The asymmetry of the PMD for a specific choice of k_z and k_y can be approximated by the shift of the maximum of the lateral distribution corresponding to finding the k_x that solves the equation

$$\frac{\partial P(\boldsymbol{k})}{\partial(\hbar k_x)} = 0. \tag{A12}$$

Solving Eq. (A12) is equivalent to solving

$$\frac{\partial {\rm Im}[S_{\rm tot}(t_s,\boldsymbol{k})]}{\partial(\hbar k_x)} = 0. \tag{A13}$$

To solve Eq. (A13), the imaginary part of $S_{\rm tot}$ needs to be found. We consider the tunneling limit $\gamma \to 0$ and consider the dominant small final momenta in the polarization direction, $|\hbar k_z| \ll E_0/\omega$. In the integral in Eq. (A7), the total phase becomes

$$S_{\rm tot}(t_s,\boldsymbol{k}) = \left[\frac{(\hbar k)^2}{2m} + I_p\right]t_s + \frac{qE_0}{m\omega^2}\cos(\omega t_s)\hbar k_z + \frac{q^2}{m}\left(1 + \frac{\hbar k_x}{mc}\right)\frac{E_0^2}{4\omega^2}\left[t_s - \frac{1}{\omega}\cos(\omega t_s)\sin(\omega t_s)\right]. \tag{A14}$$

To find the imaginary part of $S_{\rm tot}$, the quantities t_s, $\cos(\omega t_s)$, and $\sin(\omega t_s)\cos(\omega t_s)$ are expanded in orders of $\gamma_{\rm eff}$ and $(\omega/E_0)\hbar k_z$. Since the front factors on the t_s-dependent terms in Eq. (A14) are different and relate to the expansion variables, the individual t_s-dependent factors are expanded to different orders. The t_s in the term $[\frac{(\hbar k)^2}{2m} + I_p]t_s$ is expanded to first order with the result

$$t_s \approx \frac{1}{\omega}\left(\frac{\omega}{qE_0}\hbar k_x + i\gamma_{\rm eff}\right), \tag{A15}$$

from which the imaginary part is readily found.

The $\cos(\omega t_s)$ factor is expanded to second order,

$$\cos(\omega t_s) = \cos\left[\arcsin\left(\frac{\omega}{qE_0}\hbar k_z + i\gamma_{\rm eff}\right)\right] = \sqrt{1 - \left(\frac{\omega}{qE_0}\hbar k_z + i\gamma_{\rm eff}\right)^2} \approx 1 - i\frac{\omega}{qE_0}\hbar k_z\gamma_{\rm eff} - \frac{1}{2}\left(\frac{\omega}{qE_0}\right)^2(\hbar k_z)^2 + \frac{1}{2}\gamma_{\rm eff}^2, \tag{A16}$$

from where we can also read-off the imaginary part.

The t_s in the last parenthesis in the last factor in Eq. (A14) is expanded to third order,

$$t_s \approx \frac{1}{\omega}\left[\frac{\omega}{qE_0}\hbar k_x + i\gamma_{\rm eff} - i\frac{1}{6}\gamma_{\rm eff}^3 + \frac{1}{6}\left(\frac{\omega}{qE_0}\right)^3(\hbar k_z)^3 + i\frac{1}{2}\left(\frac{\omega}{qE_0}\right)^2(\hbar k_z)^2\gamma_{\rm eff} - \frac{1}{2}\frac{\omega}{qE_0}\hbar k_z\gamma_{\rm eff}^2\right], \tag{A17}$$

and one finds that the imaginary part of t_s has the following approximate expression:

$${\rm Im}(t_s) \approx \frac{1}{\omega}\left[\gamma_{\rm eff} - \frac{1}{6}\gamma_{\rm eff}^3 + \frac{1}{2}\left(\frac{\omega}{qE_0}\right)^2(\hbar k_z)^2\gamma_{\rm eff}\right]. \tag{A18}$$

Finally, the expansion of $\cos(\omega t_s)\sin(\omega t_s)$ to third order yields

$$\cos(\omega t_s)\sin(\omega t_s) = \sqrt{1 - \left(\frac{\omega}{qE_0}\hbar k_z + i\gamma_{\rm eff}\right)^2}\left(\frac{\omega}{qE_0}\hbar k_z + i\gamma_{\rm eff}\right) \approx \left[1 - i\frac{\omega}{qE_0}\hbar k_z\gamma_{\rm eff} - \frac{1}{2}\left(\frac{\omega}{qE_0}\right)^2(\hbar k_z)^2 + \frac{1}{2}\gamma_{\rm eff}^2\right]\left(\frac{\omega}{qE_0}\hbar k_z + i\gamma_{\rm eff}\right), \tag{A19}$$

with the imaginary part

$${\rm Im}[\cos(\omega t_s)\sin(\omega t_s)] \approx \gamma_{\rm eff} - \frac{3}{2}\left(\frac{\omega}{qE_0}\right)^2(\hbar k_z)^2\gamma_{\rm eff} + \frac{1}{2}\gamma_{\rm eff}^3. \tag{A20}$$

To find the k_x that solves Eq. (A13) to the first order in $1/c$, we assume that γ_{eff} is k_x independent. This approximation yields the same result as solving for a k_x-dependent γ_{eff} and expanding this solution to the first order in $1/c$. However, the considered calculation is much less tedious. The equation to solve reads

$$\begin{aligned}\frac{\partial \text{Im}[S_{\text{tot}}(t_s,\boldsymbol{k})]}{\partial(\hbar k_x)} = 0 &= \frac{\hbar k_x}{m}\gamma_{\text{eff}} + \frac{q^2}{m}\frac{1}{mc}\frac{E_0^2}{4\omega^2}\frac{1}{\omega}\left[\gamma_{\text{eff}} - \frac{1}{6}\gamma_{\text{eff}}^3 + \frac{1}{2}\left(\frac{\omega}{qE_0}\right)^2(\hbar k_z)^2\gamma_{\text{eff}}\right] \\ &\quad + \frac{q^2}{m}\frac{1}{mc}\frac{E_0^2}{4\omega^2}\frac{1}{\omega}\left[-\gamma_{\text{eff}} + \frac{3}{2}\left(\frac{\omega}{qE_0}\right)^2(\hbar k_z)^2\gamma_{\text{eff}} - \frac{1}{2}\gamma_{\text{eff}}^3\right] \\ &= \frac{\hbar k_x}{m}\gamma_{\text{eff}} + \frac{q^2}{m}\frac{1}{mc}\frac{E_0^2}{4\omega^2}\frac{1}{\omega}\left[2\left(\frac{\omega}{qE_0}\right)^2(\hbar k_z)^2\gamma_{\text{eff}} - \frac{4}{6}\gamma_{\text{eff}}^3\right],\end{aligned}$$

which implies that the nondipole-induced shift in the laser propagation direction is

$$(\hbar k_x)_{\text{shift}} = \frac{q^2}{m}\frac{1}{c}\frac{E_0^2}{4\omega^2}\left[\frac{4}{6}\left(\frac{\omega}{qE_0}\right)^2\left((\hbar k_y)^2 + 2mI_p\right) - 2\left(\frac{\omega}{qE_0}\right)^2(\hbar k_z)^2\right] = \frac{1}{c}\left[\frac{1}{3}\left(\frac{(\hbar k_y)^2}{2m} + I_p\right) - \frac{(\hbar k_z)^2}{2m}\right]. \tag{A21}$$

As seen from Eq. (A21), for the shift of maximum in the PMD, at $k_z = k_y = 0$, the shift is $\hbar k_{x,\text{shift}} = 1/(3c)I_p$. Note that the sign on the term proportional to k_z^2 is negative in the present case based on the nondipole strong-field-approximation Hamiltonian. With the full $1/c$ Hamiltonian, a similar derivation as the one above gives a positive sign on that term; see Supplemental Material of Ref. [17]. Since most of the ionization yield comes in the vicinity of the point $k_z = k_y = 0$, the total shift in momentum in the propagation direction will be in the positive direction at a distance of approximately $1/(3c)I_p$. This shift is given by Eq. (54) of the main text.

[1] M. Ilchen, G. Hartmann, E. V. Gryzlova, A. Achner, E. Allaria, A. Beckmann, M. Braune, J. Buck, C. Callegari, R. N. Coffee, R. Cucini, M. Danailov, A. De Fanis, A. Demidovich, E. Ferrari, P. Finetti, L. Glaser, A. Knie, A. O. Lindahl, O. Plekan, N. Mahne, T. Mazza, L. Raimondi, E. Roussel, F. Scholz, J. Seltmann, I. Shevchuk, C. Svetina, P. Walter, M. Zangrando, J. Viefhaus, A. N. Grum-Grzhimailo, and M. Meyer, Symmetry breakdown of electron emission in extreme ultraviolet photoionization of argon, Nat. Commun. **9**, 4659 (2018).

[2] J. W. Cooper, Multipole corrections to the angular distribution of photoelectrons at low energies, Phys. Rev. A **42**, 6942 (1990).

[3] A. Bugacov, M. Pont, and R. Shakeshaft, Possibility of breakdown of atomic stabilization in an intense high-frequency field, Phys. Rev. A **48**, R4027 (1993).

[4] J. R. Vázquez de Aldana, N. J. Kylstra, L. Roso, P. L. Knight, A. Patel, and R. A. Worthington, Atoms interacting with intense, high-frequency laser pulses: Effect of the magnetic-field component on atomic stabilization, Phys. Rev. A **64**, 013411 (2001).

[5] M. Forre and A. S. Simonsen, Nondipole ionization dynamics in atoms induced by intense xuv laser fields, Phys. Rev. A **90**, 053411 (2014).

[6] A. S. Simonsen and M. Førre, Magnetic-field-induced enhancement of atomic stabilization in intense high-frequency laser fields, Phys. Rev. A **92**, 013405 (2015).

[7] M. Førre and A. S. Simonsen, Generalized velocity-gauge form of the light-matter interaction hamiltonian beyond the dipole approximation, Phys. Rev. A **93**, 013423 (2016).

[8] A. S. Simonsen and M. Førre, Dipole-forbidden atomic transitions induced by superintense x-ray laser fields, Phys. Rev. A **93**, 063425 (2016).

[9] T. E. Moe and M. Førre, Ionization of atomic hydrogen by an intense x-ray laser pulse: An *ab initio* study of the breakdown of the dipole approximation, Phys. Rev. A **97**, 013415 (2018).

[10] H. Bachau, M. Dondera, and V. Florescu, Stimulated Compton Scattering in Two-Color Ionization of Hydrogen with keV Electromagnetic Fields, Phys. Rev. Lett. **112**, 073001 (2014).

[11] H. Bachau, M. Dondera, V. Florescu, and T. A. Marian, Stimulated raman transitions from the metastable 2s state of hydrogen, J. Phys. B **50**, 174003 (2017).

[12] H. R. Reiss, Limits on Tunneling Theories of Strong-Field Ionization, Phys. Rev. Lett. **101**, 043002 (2008).

[13] H. R. Reiss, The tunneling model of laser-induced ionization and its failure at low frequencies, J. Phys. B **47**, 204006 (2014).

[14] A. Ludwig, J. Maurer, B. W. Mayer, C. R. Phillips, L. Gallmann, and U. Keller, Breakdown of the Dipole Approximation in Strong-Field Ionization, Phys. Rev. Lett. **113**, 243001 (2014).

[15] C. T. L. Smeenk, L. Arissian, B. Zhou, A. Mysyrowicz, D. M. Villeneuve, A. Staudte, and P. B. Corkum, Partitioning of the Linear Photon Momentum in Multiphoton Ionization, Phys. Rev. Lett. **106**, 193002 (2011).

[16] N. Haram, I. Ivanov, H. Xu, K. T. Kim, A. Atia-tul Noor, U. S. Sainadh, R. D. Glover, D. Chetty, I. V. Litvinyuk, and R. T. Sang, Relativistic Nondipole Effects in Strong-Field Atomic Ionization at Moderate Intensities, Phys. Rev. Lett. **123**, 093201 (2019).

[17] A. Hartung, S. Eckart, S. Brennecke, J. Rist, D. Trabert, K. Fehre, M. Richter, H. Sann, S. Zeller, K. Henrichs, G. Kastirke, J. Hoehl, A. Kalinin, M. S. Schöffler, T. Jahnke, L. Ph. H. Schmidt, M. Lein, M. Kunitski, and R. Dörner, Magnetic fields alter strong-field ionization, Nat. Phys. **15**, 1222 (2019).

[18] M. Klaiber, E. Yakaboylu, H. Bauke, K. Z. Hatsagortsyan, and C. H. Keitel, Under-the-Barrier Dynamics in Laser-Induced Relativistic Tunneling, Phys. Rev. Lett. **110**, 153004 (2013).
[19] E. Yakaboylu, M. Klaiber, H. Bauke, K. Z. Hatsagortsyan, and C. H. Keitel, Relativistic features and time delay of laser-induced tunnel ionization, Phys. Rev. A **88**, 063421 (2013).
[20] S. Chelkowski, A. D. Bandrauk, and P. B. Corkum, Photon Momentum Sharing between an Electron and an Ion in Photoionization: From One-Photon (Photoelectric Effect) to Multiphoton Absorption, Phys. Rev. Lett. **113**, 263005 (2014).
[21] S. Chelkowski, A. D. Bandrauk, and P. B. Corkum, Photon-momentum transfer in multiphoton ionization and in time-resolved holography with photoelectrons, Phys. Rev. A **92**, 051401(R) (2015).
[22] S. Chelkowski and A. D. Bandrauk, Photon momentum transfer in photoionisation: Unexpected breakdown of the dipole approximation, Mol. Phys. **115**, 1971 (2017).
[23] T. Keil and D. Bauer, Coulomb-corrected strong-field quantum trajectories beyond dipole approximation, J. Phys. B **50**, 194002 (2017).
[24] P.-L. He, D. Lao, and F. He, Strong Field Theories beyond Dipole Approximations in Nonrelativistic Regimes, Phys. Rev. Lett. **118**, 163203 (2017).
[25] S. Chelkowski and A. D. Bandrauk, Photon-momentum transfer in molecular photoionization, Phys. Rev. A **97**, 053401 (2018).
[26] S. Brennecke and M. Lein, High-order above-threshold ionization beyond the electric dipole approximation: Dependence on the atomic and molecular structure, Phys. Rev. A **98**, 063414 (2018).
[27] S. Brennecke and M. Lein, High-order above-threshold ionization beyond the electric dipole approximation, J. Phys. B **51**, 094005 (2018).
[28] B. Willenberg, J. Maurer, U. Keller, J. Daněk, M. Klaiber, N. Teeny, K. Z. Hatsagortsyan, and C. H. Keitel, Holographic interferences in strong-field ionization beyond the dipole approximation: The influence of the peak and focal-volume-averaged laser intensities, Phys. Rev. A **100**, 033417 (2019).
[29] S. Brennecke and M. Lein, Strong-field photoelectron holography beyond the electric dipole approximation: A semiclassical analysis, Phys. Rev. A **100**, 023413 (2019).
[30] B. Böning, W. Paufler, and S. Fritzsche, Nondipole strong-field approximation for spatially structured laser fields, Phys. Rev. A **99**, 053404 (2019).
[31] L. B. Madsen, Gauge invariance in the interaction between atoms and few-cycle laser pulses, Phys. Rev. A **65**, 053417 (2002).
[32] M. D Feit, J. A Fleck, and A Steiger, Solution of the Schrödinger equation by a spectral method, J. Comput. Phys. **47**, 412 (1982).
[33] H. B. van Linden van den Heuvell and H. G. Muller, in *Multiphoton Processes*, edited by S. J. Smith and P. L. Knight (Cambridge University Press, Cambridge, 1988).
[34] T. F. Gallagher, Above-Threshold Ionization in Low-Frequency Limit, Phys. Rev. Lett. **61**, 2304 (1988).
[35] P. B. Corkum, N. H. Burnett, and F. Brunel, Above-Threshold Ionization in the Long-Wavelength Limit, Phys. Rev. Lett. **62**, 1259 (1989).
[36] K. C. Kulander, K. J. Schafer, and J. L. Krause, in *Super-Intense Laser-Atom Physics*, edited by B. Piraux, A. L'Hullier, and K. Rzazewski (Plenum, New York, 1993).
[37] P. B. Corkum, Plasma Perspective on Strong Field Multiphoton Ionization, Phys. Rev. Lett. **71**, 1994 (1993).
[38] S. P. Goreslavski, G. G. Paulus, S. V. Popruzhenko, and N. I. Shvetsov-Shilovski, Coulomb Asymmetry in Above-Threshold Ionization, Phys. Rev. Lett. **93**, 233002 (2004).
[39] N. I. Shvetsov-Shilovski, D. Dimitrovski, and L. B. Madsen, Ionization in elliptically polarized pulses: Multielectron polarization effects and asymmetry of photoelectron momentum distributions, Phys. Rev. A **85**, 023428 (2012).
[40] M. Førre, J. P. Hansen, L. Kocbach, S. Selstø, and L. B. Madsen, Nondipole Ionization Dynamics of Atoms in Superintense High-Frequency Attosecond Pulses, Phys. Rev. Lett. **97**, 043601 (2006).
[41] L. V. Keldysh, Ionization in the field of a strong electromagnetic wave, Zh. Eksp. Teor. Fiz. **47**, 1945 (1964) [Sov. Phys. JETP **20**, 1307 (1965)].
[42] F. H. M. Faisal, Multiple absorption of laser photons by atoms, J. Phys. B **6**, L89 (1973).
[43] H. R. Reiss, Effect of an intense electromagnetic field on a weakly bound system, Phys. Rev. A **22**, 1786 (1980).
[44] J. J. Sakurai, *Modern Quantum Mechanics* (Addison-Wesley Publishing Company, Reading, MA, 1994).
[45] L. B. Madsen, Strong-field approximation in laser-assisted dynamics, Am. J. Phys. **73**, 57 (2005).
[46] R. Kanya, Y. Morimoto, and K. Yamanouchi, Observation of Laser-Assisted Electron-Atom Scattering in Femtosecond Intense Laser Fields, Phys. Rev. Lett. **105**, 123202 (2010).
[47] Y. Morimoto, R. Kanya, and K. Yamanouchi, Laser-assisted electron diffraction for femtosecond molecular imaging, J. Chem. Phys. **140**, 064201 (2014).
[48] A. Weingartshofer, J. K. Holmes, G. Caudle, E. M. Clarke, and H. Krüger, Direct Observation of Multiphoton Processes in Laser-Induced Free-Free Transitions, Phys. Rev. Lett. **39**, 269 (1977).
[49] N. M. Kroll and K. M. Watson, Charged-particle scattering in the presence of a strong electromagnetic wave, Phys. Rev. A **8**, 804 (1973).
[50] F. V. Bunkin and M. V. Fedorov, Bremsstrahlung in a strong radiation field, Zh. Eksp. Teor. Fiz. **49**, 1215 (1966) [Sov. Phys. JETP **22**, 844 (1966)].
[51] B. Wallbank and J. K. Holmes, Laser-assisted elastic electron-atom collisions, Phys. Rev. A **48**, R2515 (1993).
[52] B. Wallbank and J. K. Holmes, Laser-assisted elastic electron-atom collisions: Low electron energy and small scattering angle, J. Phys. B **27**, 1221 (1994).
[53] B. Wallbank and J. K. Holmes, Differential cross sections for laser-assisted elastic electron scattering from argon, J. Phys. B **27**, 5405 (1994).
[54] L. B. Madsen and K. Taulbjerg, Theory of laser-assisted electron-atom scattering: Beyond the Kroll-Watson approximation, J. Phys. B **28**, 5327 (1995).
[55] B. Wallbank and J. K. Holmes, Laser-assisted elastic electron scattering from helium, Can. J. Phys. **79**, 1237 (2001).
[56] M. O. Musa, A. MacDonald, L. Tidswell, J. Holmes, and B. Wallbank, Laser-induced free–free transitions in elastic

electron scattering from CO_2, J. Phys. B **43**, 175201 (2010).

[57] T. E. Glover, R. W. Schoenlein, A. H. Chin, and C. V. Shank, Observation of Laser Assisted Photoelectric Effect and Femtosecond High Order Harmonic Radiation, Phys. Rev. Lett. **76**, 2468 (1996).

[58] J. Itatani, F. Quéré, G. L. Yudin, M. Yu. Ivanov, F. Krausz, and P. B. Corkum, Attosecond Streak Camera, Phys. Rev. Lett. **88**, 173903 (2002).

[59] J. C. Baggesen and L. B. Madsen, Polarization Effects in Attosecond Photoelectron Spectroscopy, Phys. Rev. Lett. **104**, 043602 (2010).